

Syndromic deafness gene ATP6V1B2 controls degeneration of spiral ganglion neurons through modulating proton flux

Shiwei Qiu (✉ 18361337211@163.com)

PLAGH: Chinese PLA General Hospital <https://orcid.org/0000-0003-1474-6957>

Weihao Zhao

Chinese PLA General Hospital

Xue Gao

PLA Rocket Force Characteristic Medical Center

Dapeng Li

NIBS: National Institute of Biological Sciences

Weiqian Wang

Chinese PLA General Hospital

Bo Gao

Chinese PLA General Hospital

Weiju Han

Chinese PLA General Hospital

Shiming Yang

Chinese PLA General Hospital

Pu Dai

Chinese PLA General Hospital

Peng Cao

NIBS: National Institute of Biological Sciences

Yongyi Yuan

Chinese PLA General Hospital <https://orcid.org/0000-0002-7936-4776>

Research Article

Keywords: Syndromic hearing loss, Atp6v1b2, lysosome, apoptosis, function compensation

Posted Date: April 26th, 2021

DOI: <https://doi.org/10.21203/rs.3.rs-452428/v1>

License:  This work is licensed under a Creative Commons Attribution 4.0 International License.

[Read Full License](#)

Abstract

ATP6V1B2 encodes the V1B2 subunit in V-ATPase, a proton pump responsible for the acidification of lysosomes. Mutations in this gene cause DDOD syndrome, DOORS syndrome, and Zimmermann-Laband syndrome, which share overlapping features of congenital sensorineural deafness, onychodystrophy, and different extents of intellectual disability without or with epilepsy. However, the underlying mechanism is unclear. To investigate the pathological role of mutant *ATP6V1B2* in the auditory system, we evaluated auditory brainstem response, distortion product otoacoustic emissions, in a transgenic line of mice carrying c.1516 C > T (p.Arg506*) in *Atp6v1b2*, *Atp6v1b2*^{Arg506*/Arg506*}. To explore the pathogenic mechanism of neurodegeneration in the auditory pathway, immunostaining, western blotting, and RNAscope analyses were performed in *Atp6v1b2*^{Arg506*/Arg506*} mice. The *Atp6v1b2*^{Arg506*/Arg506*} mice showed hidden hearing loss at early stages and developed late-onset hearing loss. We observed increased transcription of *Atp6v1b1* in hair cells of *Atp6v1b2*^{Arg506*/Arg506*} mice and inferred that *Atp6v1b1* compensated for the *Atp6v1b2* dysfunction by increasing its own transcription level. Genetic compensation in hair cells explains the milder hearing impairment in *Atp6v1b2*^{Arg506*/Arg506*} mice. Apoptosis activated by lysosomal dysfunction and the subsequent blockade of autophagic flux induced the degeneration of spiral ganglion neurons and further impaired the hearing. Intraperitoneal administration of the apoptosis inhibitor, BIP-V5, improved both phenotypical and pathological outcomes in two live mutant mice. Based on the pathogenesis underlying hearing loss in *ATP6V1B2*-related syndromes, systemic drug administration to inhibit apoptosis might be an option for restoring the function of spiral ganglion neurons and promoting hearing, which provides a direction for future treatment.

Introduction

V-ATPase is a multi-subunit enzyme complex also known as the vacuolar H⁺-ATPase. This proton pump is mainly responsible for the acidification of lysosomes and other membrane-bound compartments (Beyenbach and Wieczorek 2006). V-ATPase comprises a peripheral V1 domain catalyzing ATP hydrolysis and a membrane integral V0 domain involved in proton translocation (Beyenbach and Wieczorek 2006; Mindell 2012). The V1 domain includes at least eight different subunits (A-H), while the V0 domain includes six different subunits (a, d, e, c, c', and c''). The loss of any subunit will disrupt the assembly of V-ATPase and affect lysosome acidification, which could lead to various disorders (Ma et al. 2011).

ATP6V1B2, which encodes the V1B2 subunit in V-ATPase, is the causative gene for dominant deafness-onychodystrophy syndrome (DDOD syndrome, MIM: 124480) (Yuan et al. 2014); deafness, onychodystrophy, osteodystrophy, intellectual disability, and seizures syndrome (DOORS syndrome, MIM: 220500) (Beauregard-Lacroix et al. 2020); and Zimmermann-Laband syndrome (ZLS, MIM: 135500) (Kortum et al. 2015). These syndromes share the symptoms of congenital sensorineural deafness, onychodystrophy, and different extents of intellectual disability without or with epilepsy. *ATP6V1B2*

c.1516 C > T, p.Arg506*, was identified in all families with DDOD syndrome (Menendez et al. 2017; Yuan et al. 2014). To investigate the pathological role of mutant *ATP6V1B2* in the neurosensory system, we generated a transgenic line of mice carrying c.1516 C > T (p.Arg506*) in *Atp6v1b2*, *Atp6v1b2*^{Arg506*/Arg506*} (homozygous mutant), and identified that the mutant mice displayed obvious cognitive defects for which impairment in the hippocampal CA1 region might be the pathological basis (Zhao et al. 2019). The interaction between the V1B2 and V1E subunits was found to be weaker in *Atp6v1b2*^{Arg506*/Arg506*} mice than in wildtype (WT) mice, indicating that the assembly of V-ATPase was affected by the mutation (Zhao et al. 2019). In another prior study, when pIRES2-EGFP-*ATP6V1B2* WT and pIRES2-EGFP-*ATP6V1B2* c.1516 C > T mutant plasmids were transfected into HEK293 cells, the lysosomal pH was increased, revealing the reduced acidification in the lysosome caused by the c.1516 C > T mutation (Yuan et al. 2014). Lysosomes, as scavengers of living cells, play a critical role in cellular metabolism. An abnormal lysosomal pH will cause dysfunctional macromolecule degradation and lead to lysosomal storage diseases. Loss of the V-ATPase subunits in the *Drosophila* fat body cells resulted in an abnormal pH in the lysosomal lumen, causing an accumulation of nonfunctional lysosomes and leading to a blockade of autophagic flux (Mauvezin et al. 2015). Additionally, abnormalities in autophagy caused by V-ATPase defects are associated with neurodegenerative diseases (Cerri and Blandini 2019; Peric and Annaert 2015).

Whether the *Atp6v1b2* c.1516 C > T mutation results in autophagic dysfunction and leads to abnormal auditory function remains unanswered. However, the *Atp6v1b2*^{Arg506*/Arg506*} mice displayed normal auditory brainstem response (ABR) thresholds before 24 weeks of age (Zhao et al. 2019), while in the patients with *ATP6V1B2*-related syndromes, the hearing loss is congenital and severe. Genetic compensation can be induced by nonsense mutations that could occur between homologous genes (Ma et al. 2019). Two highly homologous genes encode V1B subunits: *ATP6V1B1* and *ATP6V1B2*. The B2 subunit of V-ATPase was shown to functionally substitute for the B1 subunit (Paunescu et al. 2007). Therefore, we speculate that genetic compensation might be responsible for the phenotype of *Atp6v1b2*^{Arg506*/Arg506*} mice.

Herein, we performed long-term studies on hearing in *Atp6v1b2*^{Arg506*/Arg506*} mice, investigated the pathogenic mechanism of neurodegeneration in the auditory pathway, and confirmed the genetic compensation in *Atp6v1b2*^{Arg506*/Arg506*} mice to explain the difference between hearing impairments observed in patients and those produced in this mouse model.

Materials And Methods

Animals

Atp6v1b2^{Arg506*/Arg506*} mice were generated in the C57BL/6 strain background by Shanghai Model Organisms Center, Inc. (Shanghai, China), as described in detail previously (Zhao et al. 2019).

Heterozygous (HE) mutant mice were crossed to generate homozygous *Atp6v1b2*^{Arg506*/Arg506*} (HO) mutant mice, and wildtype (WT) littermates were used as controls.

All in vivo experiments were carried out in accordance with CALAS (Chinese Association for Laboratory Animal Science) guidelines and approved by the institutional animal care and use committee of the Chinese PLA General Hospital, the Shanghai Biomodel Organism Science & Technology Development Co. Ltd., and NIBS (National Institute of Biological Sciences), Beijing.

Bax inhibitor peptide V5 (BIP-V5) treatment

The concentration of BIP-V5 was adjusted to 100 µmol/L with saline. Starting from 4 weeks after birth, mice (n = 8) were injected intraperitoneally at a dose of 10 µL/g body weight once weekly until 40 weeks after birth. In addition, WT (n = 8) and *Atp6v1b2*^{Arg506*/Arg506*} (n = 8) control mice were injected intraperitoneally with saline alone.

ABR analysis

Hearing was evaluated in WT and *Atp6v1b2*^{Arg506*/Arg506*} mice at the age of 4, 12, 20, 28, 36, and 40 weeks (n = 6 per genotype and age group). In brief, the stimuli of ABR included click and tone-burst (1, 2, 4, 8, 16, 24, and 32 kHz) and were presented from 90 to 10 dB SPL. Amplitude and latency of ABR wave I were analyzed for 90 dB SPL click stimuli.

Distortion product otoacoustic emissions (DPOAE) analysis

The intensity and frequency of the original sounds were set as f1 and f2, respectively. The sound frequency range was set as 4–32 kHz. Each frequency had 200 superposition times. The amplitude of 2f1-f2 frequency was considered the observation index, and the signal-to-noise ratio of DPOAE at each frequency was calculated by the BioSigRZ software. The threshold that DPOAE can derive was set to be at least 6 dB SPL above the baseline noise.

Immunostaining

Inner ear tissues were dissected and fixed in 4% paraformaldehyde for 1–2 h at room temperature or for 12 h at 4°C, followed by decalcification in 10% EDTA (pH = 7.2) at 4°C for 5 days. For cryosections, the calcium-depleted cochlea tissues were placed into a 30% sucrose solution for dehydration. Serial sections were cut at 10 µm thickness. For basilar membrane with organ of Corti, cochlea ducts were dissected.

The primary antibodies used were as follows: rabbit anti-Myo7a (Proteus Biosciences, Ramona, CA, 1:300), mouse anti-Ctbp2 (BD Biosciences, San Jose, CA, 1:200), chicken anti-NFH (AB5539, EMD Millipore, Billerica, 1:500), rabbit anti-beta III tubulin (ab230847, Abcam, UK, 1:500), rabbit anti-cleaved caspase-3 (9661, Cell Signaling Technology, Boston, MA, 1:500), rat anti-MBP (MAB386, EMD Millipore, Billerica, MA, 1:500), rabbit anti-caspase-3 (ab4051, Abcam, UK, 1:500), rat anti-LAMP1 (ab25245, Abcam, UK, 1:500), rabbit anti-Bax (ab199677, Abcam, UK, 1:500), rabbit anti-BCL2 (12789-1-AP, Proteintech, Chicago, IL, 1:500), rabbit anti-LC3B (ab48394, Abcam, UK, 1:500), rabbit anti-TOM20 (SC-11415, CiteAB,

Santa Cruz, 1:500), and mouse anti-cytochrome C (556432, BD Pharmingen, USA). The secondary antibodies used were as follows: goat anti-rabbit IgG (A-11008, Thermo Fisher Scientific, Waltham, MA, 1:500), goat anti-mouse IgG (A-10684, Thermo Fisher Scientific, Waltham, MA, 1:500), goat anti-rat IgG (A-11077, Thermo Fisher Scientific, Waltham, MA, 1:500), and goat anti-chicken IgY (A-21449, Thermo Fisher Scientific, Waltham, MA, 1:500). Nuclei were labelled with DAPI.

Confocal laser scanning microscopy

Confocal z-stacks (0.3 μm step size) of cochlea tissues were taken using either a Zeiss LSM800 or a Leica SP8 microscope. ImageJ software (version 1.46, NIH, MD) was used for image processing of z-stacks. All immunofluorescence images shown in this study are representative of at least three individual mice in each group.

Western blotting

The cochlea tissues were quickly removed from mice and cryo-milled in RIPA lysis buffer and centrifuged. The supernatants were collected, and the protein concentration was detected using the BCA protein assay kit (PI23227, Thermo Fisher Scientific, Waltham, MA). Then equal amounts of protein sample were separated by 12% Tris/Glycine SDS-PAGE and transferred to a polyvinylidene difluoride membrane. The primary antibodies used were the same as those used for immunostaining analysis. The experiments were independently repeated three times.

Transmission electron microscopy (TEM)

Mice were perfused intracardially with 4% paraformaldehyde (in 0.1 M phosphate buffer). Cochleae were then isolated and postfixed with 1.5% paraformaldehyde and 2.5% glutaraldehyde, followed by decalcification in 10% EDTA at 4°C for 5 days and osmification in 1% osmium tetroxide. Then the samples were dehydrated in ethanol and embedded in araldite resin. After resin solidification, semi-thin sections were made stained for localization. Then ultra-thin sections, uranium dioxide acetate saturated and lead citrate were stained respectively. TEM was performed using a Jeol 1400-plus electron microscope (JEM-1400, JEDL, Tokyo). Multiple non-overlapping regions of the ANF cross-sections were imaged at $\times 3,400$ magnification. All images of semi-thin sections and electron microscope sections shown are representative of at least three individual mice in each group.

RNAscope

Cochleae of 4-week-old mice were perfused and decalcified. After freezing the tissues in OCT compound with dry ice or liquid nitrogen, they were stored in an airtight container at -80°C . Before tissue sectioning, the tissue blocks were placed at -20°C for at least 1 h in a cryostat. The blocks were then sectioned to 7 μm . After air drying the slides for 20 min at -20°C , the RNAscope experiment was performed as previously described (Shrestha et al. 2018; Sun et al. 2018). The following probes for RNA binding were used: Mm-Atp6v1b1 (#804281, Advanced Cell Diagnostics, USA) and Mm-Atp6v1b1-C2 (#804291-C2, Advanced Cell Diagnostics). The sections were imaged using a confocal microscope.

Statistical analysis

Statistical analyses were performed using Microsoft Excel and SPSS (18.0). Statistical differences were analyzed using t-test. The data are represented as the mean \pm SEM. Densitometric analysis in the western blotting experiment was performed using the ImageJ software. P values less than 0.05 were considered to indicate statistical significance.

Results

Atp6v1b2^{Arg506*/Arg506*} mice begin to develop hidden hearing loss (HHL) at 12 weeks and develop hearing loss at 28 weeks after birth

Mice were phenotyped using ABR at 4–40 weeks of age. The ABR waveform in mice is composed of five peaks, corresponding to electrical signals generated by different components of the peripheral auditory pathway (Fig. 1A). The ABR at 4, 20, and 40 weeks, which represent the early, middle, and aged stages of *Atp6v1b2*^{Arg506*/Arg506*} mice, are shown in Figs. 1B-1D. The ABR of the mice at other ages are shown in Figures S1A-S1C. The thresholds for *Atp6v1b2*^{Arg506*/Arg506*} mice did not differ significantly from those of WT mice at 4, 12, and 20 weeks. *Atp6v1b2*^{Arg506*/Arg506*} mice presented HHL at 12 and 20 weeks with lower P1 amplitudes and a longer latency than WT mice (Figs. 1C, 1D, S1B, S1C). From 28 weeks, *Atp6v1b2*^{Arg506*/Arg506*} mice showed progressive HL and increased ABR thresholds compared with WT mice (70 dB SPL average, Figure S1A). However, DPOAE analysis showed no significant difference between *Atp6v1b2*^{Arg506*/Arg506*} and WT mice, which indicated the normal function of outer hair cells (OHCs).

No morphological changes of the organ of Corti between WT and *Atp6v1b2*^{Arg506*/Arg506*} mice were observed (Fig. 2B), also indicating that hearing loss in *Atp6v1b2*^{Arg506*/Arg506*} mice was not related to hair cell loss. The synaptic density in *Atp6v1b2*^{Arg506*/Arg506*} mice did not differ significantly from that in WT mice at different ages (Figure S2). Interestingly, although the auditory nerve fibers of *Atp6v1b2*^{Arg506*/Arg506*} mice did not change significantly at 4 weeks, the myelin sheath covering the auditory nerve fibers decreased at 20 weeks (Fig. 2C, 2D). We labeled the unmyelinated nerve fibers in the osseous spiral lamina (OSL) of mouse cochlea with the NFH antibody (Figures S3A-S3F). In the cochlea of *Atp6v1b2*^{Arg506*/Arg506*} mice at 20 weeks, parts of auditory nerve fibers in the OSL stained positive for NFH, indicating the presence of auditory nerve fiber demyelination (Figure S3F, S3C), which was consistent with myelin stain results (Fig. 2C, Fig. 2D). To further clarify the changes in myelination of the nerve fibers, we performed TEM to observe the morphology of the myelin sheath in mice at 4, 12, and 20 weeks of age (Figure S3G-L). *Atp6v1b2*^{Arg506*/Arg506*} mice showed vacuolar-like changes in the myelin sheath of auditory nerve fibers in the OSL at 4 weeks, but the myelin sheath was still wrapped around the nerve fibers (Figure S3J). Demyelination was observed in the auditory nerve fibers of *Atp6v1b2*^{Arg506*/Arg506*} mice at 12 and 20 weeks (Figure S3K, S3L). These changes did not appear in WT mice (Figures S3G-S3I). The above results indicate that demyelination of cochlear auditory nerve fibers was the pathological basis for HHL in *Atp6v1b2*^{Arg506*/Arg506*} mice.

In addition, the number of SGNs decreased significantly in *Atp6v1b2*^{Arg506*/Arg506*} mice compared to that in WT mice at 40 weeks (Fig. 2E, 2F). The excitation of type I SGNs is caused by the action potential of IHCs and is further transmitted to the neuronal body, type II SGNs connect the OHCs and are mainly responsible for receiving signals from the OHCs (Fig. 2A). Another special feature of type II SGNs is that the cell bodies and the nerve fibers that connect the OHCs are unmyelinated. By labeling type II nerve fibers with NFH antibody, we found that the number of type II nerve fibers connecting the OHCs was reduced in *Atp6v1b2*^{Arg506*/Arg506*} mice at 28 weeks (Figure S1D, S1E). In summary, the decrease in SGNs was the cause of hearing loss in the aged *Atp6v1b2*^{Arg506*/Arg506*} mice.

Atp6v1b2 c.1516C > T causes abnormal autophagy, which leads to apoptosis of the SGNs in *Atp6v1b2*^{Arg506*/Arg506*} mice

Western blotting results revealed increased LC3-II in the cochlea of *Atp6v1b2*^{Arg506*/Arg506*} mice (Fig. 3B), indicating that autophagosomes accumulated in the cytoplasm. In *Atp6v1b2*^{Arg506*/Arg506*} mice, autophagosomes increased in the SGNs (Fig. 3A). However, in the organ of Corti, there was no significant difference between WT and *Atp6v1b2*^{Arg506*/Arg506*} mice (Figure S4A). To evaluate if this increase in autophagosomes in the SGNs could be explained by a fusion barrier between autophagosomes and lysosomes or the abnormal degradation of the lysosome, we performed TEM analysis. The results showed high levels of substrates in the autophagic lysosomes of the SGNs in *Atp6v1b2*^{Arg506*/Arg506*} mice (Fig. 4A), indicating that autophagosomes could fuse with the lysosomes. However, the proportion of autolysosomes increased in the SGNs of *Atp6v1b2*^{Arg506*/Arg506*} mice (Fig. 4B), suggesting that the substrates in the lysosomal cavity could not be effectively degraded, which further made it difficult for autophagosomes to enter lysosomes. Thus, we speculated that abnormal lysosomal degradation was the cause of the autophagosome accumulation in the cytoplasm of the SGNs.

Immunofluorescence analysis revealed that cytochrome C was released from the mitochondria to the cytosol of the SGNs of *Atp6v1b2*^{Arg506*/Arg506*} mice (Fig. 3C). Western blotting results showed that in the cochlea of *Atp6v1b2*^{Arg506*/Arg506*} mice, the ratio of Bcl-2 to Bax was reduced significantly compared with that in WT mice (Fig. 3D). Results showed that cleaved caspase-3 in the inner ear of *Atp6v1b2*^{Arg506*/Arg506*} mice increased significantly (Fig. 3F). To further verify the exact area of apoptosis, immunofluorescence staining was performed. The results showed that in the cochlea of *Atp6v1b2*^{Arg506*/Arg506*} mice, apoptosis was mostly observed in the spiral ganglia (Fig. 3E), and no excessive apoptosis was identified in the organ of Corti (Figure S4C).

These data suggested that in the inner ear of *Atp6v1b2*^{Arg506*/Arg506*} mice, disequilibrium of the acidic environment in the lysosomes and autophagosome accumulation in the cytoplasm led to a decrease in the ratio of Bcl-2 to Bax, which further increased the outer membrane permeability of the mitochondria and induced the release of cytochrome C and activation of caspase-3.

BIP-V5 improves phenotypical and pathological outcomes in *Atp6v1b2*^{Arg506*/Arg506*} mice

During the process of BIP-V5 administration, four mice in the *Atp6v1b2*^{Arg506*/Arg506*}-BIP-V5 group died, thus affecting the statistics of the experimental data. We observed that the hearing threshold was restored in two out of four *Atp6v1b2*^{Arg506*/Arg506*} mice treated with BIP-V5, and they had better ABR waveforms (Figure S5), suggesting a potential role of BIP-V5 in improving the hearing of mutant mice. After BIP-V5 intervention, the expression of Bax (Figure S6) and the release of cytochrome C (Figure S7C) in the mitochondria of the cochlea were significantly reduced. In addition, immunostaining and western blotting results showed that active caspase-3 (Figure S6, S7D) in the cochlea of *Atp6v1b2*^{Arg506*/Arg506*} mice was reduced and the number of SGNs (Figure S7A) increased significantly with BIP-V5 intervention, but lysosomal function evaluated by autophagosomes was not significantly changed (Figure S6, S7B).

Genetic compensation exists in the hair cells of *Atp6v1b2*^{Arg506*/Arg506*} mice

Clinically, patients diagnosed with *ATP6V1B2*-related syndromes have congenital severe to profound sensorineural hearing loss; however, the hearing of *Atp6v1b2*^{Arg506*/Arg506*} mice was quite different. To verify whether functional compensation occurs in the cochlea of *Atp6v1b2*^{Arg506*/Arg506*} mice, we determined the *Atp6v1b2* and *Atp6v1b1* transcription levels and localization in the cochlea of mice at 4 weeks by RNAscope and found that the RNA level of *Atp6v1b2* was downregulated in both the SGNs and hair cells in *Atp6v1b2*^{Arg506*/Arg506*} mice compared with that in WT mice, indicating that the transcription level of *Atp6v1b2* decreased or that the RNA was excessively degraded. In *Atp6v1b2*^{Arg506*/Arg506*} mice, the transcription level of *Atp6v1b1* significantly increased in the hair cells but not in the SGNs. These results suggested that *Atp6v1b1* may compensate for the loss of *Atp6v1b2* function in the hair cells (Fig. 5).

Discussion

The manifestation of normal auditory thresholds but reduced suprathreshold amplitude of the sound-evoked compound action potential of SGNs, shown as peak I of the ABR waveform, is defined as HHL (Bharadwaj et al. 2014; Kujawa and Liberman 2009; Mehraei et al. 2016). The pathological mechanisms of HHL are complicated and are not yet fully understood. The electrophysiological results showed that *Atp6v1b2*^{Arg506*/Arg506*} mice younger than 20 weeks did not have an elevated ABR threshold but had lower P1 amplitudes and longer P1 latencies than WT mice, similar to patients with HHL (Mehraei et al. 2016). Current studies suggest that risk factors associated with HHL include a noisy environment (Liu et al. 2019), aging (Fischer et al. 2019), and ototoxic drugs (Liu et al. 2015). LOHL is defined as hearing loss that is not present at birth but is identified at a later period. Both environmental and hereditary factors influence the development of LOHL. Clinically, there is no early diagnostic indicator for LOHL until hearing loss is detected. HHL and LOHL are regarded as two diseases with different pathogeneses (Song et al.

2019). We proposed that 1) the *Atp6v1b2*^{Arg506*/Arg506*} mouse model could be used as a natural model for HHL and LOHL; 2) patients with LOHL may have HHL early in life, and it is important for those who have been diagnosed with HHL to be cautious of risk factors such as noise, ototoxic drugs, *etc.* to avoid further hearing impairment.

Abnormalities in ribbon synaptic density and demyelination of the auditory nerve fibers have been identified as causes of HHL (Liberman and Kujawa 2017; Wan and Corfas 2017). In our study, we identified that HHL in *Atp6v1b2*^{Arg506*/Arg506*} mice was caused by demyelination of nerve fibers but not the ribbon synaptic density. Schwann cells are essential for the formation of nodes of Ranvier, which is a special structure along the myelinated fibers where voltage-gated sodium channels and potassium channels accumulate for regeneration of action potentials and fast synchronous transmission of electrical signals. This phenomenon explains why nerve fibers with myelin sheaths can conduct action potentials more quickly and efficiently than nerve fibers without myelin sheaths (Rasband and Peles 2015).

Damage or loss of cells from the auditory pathway in the cochlea, such as IHCs and/or OHCs and SGNs, is a pathological feature of LOHL (Vreugde et al. 2002). Hair cells are highly specialized cells attached to the basement membrane in the organ of Corti in the cochlea. These cells have hair-like protrusions (stereocilia) embedded in the tectorial membrane. Incoming soundwaves distort the basement membrane, and the resulting mechanical distortion of the stereocilia is transduced into neural signals that are conveyed through the SGNs to the auditory regions of the brain. Initially, *Atp6v1b2*^{Arg506*/Arg506*} mice developed demyelination of nerve fibers, followed by loss of nerve fibers and SGN cell bodies. This process appears to be neurodegenerative. However, the cochlear hair cells of *Atp6v1b2*^{Arg506*/Arg506*} mice were morphologically normal.

HL in patients with DDOD syndrome is primarily treated by cochlear implantation. However, although the implanted cochlea worked well, clinical follow-up of DDOD syndrome patients with cochlear implantation revealed that their language rehabilitation was unsatisfactory. Our findings regarding the pathological changes in SGNs and mild learning and memory problems in DDOD syndrome patients (Zhao et al. 2019) could explain this clinical puzzle.

V-ATPase has two main effects on the organelle: maintaining the acidic environment of the organelles and participating in and regulating the fusion between vesicle-type organelles, such as the fusion between lysosomes and autophagosomes (Colacurcio and Nixon 2016). We have demonstrated that abnormalities in the assembly of the subunits of V-ATPase occurred in *Atp6v1b2*^{Arg506*/Arg506*} mice, which affects the transfer of hydrogen ions into the lysosome (Yuan et al. 2014; Zhao et al. 2019). In this study, we observed the presence of metabolic substrates inside lysosomes, which indicated there might be no fusion barrier between lysosomes and autophagosomes in *Atp6v1b2*^{Arg506*/Arg506*} mice. The degradation of lysosomes depends on the presence of multiple hydrolases, and the activity of these hydrolases requires an acidic environment (De Duve 1957; Saftig and Haas 2016). We found abnormal degradation of metabolic substrates in lysosomes of the SGNs in *Atp6v1b2*^{Arg506*/Arg506*} mice as a result

of the abnormal acidic environment and the affected activity of the hydrolases in the lysosomes. In addition, redundant autophagosomes were observed outside the lysosomes in the SGNs of *Atp6v1b2*^{Arg506*/Arg506*} mice, indicating that high levels of undegraded substrates in the lysosomes affected the normal process of autophagic flow (Colacurcio and Nixon 2016).

We observed an increase in caspase-3, the ultimate initiator of apoptosis, in the SGNs and Schwann cells of *Atp6v1b2*^{Arg506*/Arg506*} mice, which suggested that lysosomal dysfunction induced apoptosis. Mitochondrial dysfunction and premature termination of cell cycle occur when a series of lysosomal functional abnormalities present, such as increased intraluminal pH value, abnormal degradation, and excessive accumulation of exogenous substrate for lysosomes (Hughes and Gottschling 2012; Molin and Demir 2014; Ruckenstuhl et al. 2014). Cell damage triggers degradation of the Bcl-2 family of proteins, which in turn activates Bax. Activated Bax/Bak complexes bind to and reduce the permeability of the mitochondrial membrane, resulting in cytochrome C release to the cytosol. Cytochrome C induces apoptosome formation, which can directly activate caspase-3 (Galluzzi et al. 2012; Ilmarinen et al. 2014; Kroemer et al. 2007).

Next, we evaluated whether treatment with the Bax inhibitor BIP-V5 could ameliorate the hearing loss in the mutant mice. After 36-week systemic administration of BIP-V5, auditory function and pathological changes improved in two out of four *Atp6v1b2*^{Arg506*/Arg506*}-BIP-V5 mice, which further verifies that apoptosis induces the degeneration of SGNs and further impaired the hearing. As the reason for mortality was unknown in 50% (four out of eight) of the treated mice, the safety of BIP-V5 treatment needs further exploration.

Patients with *ATP6V1B2*-related syndromes showed severe congenital sensorineural hearing loss, which was not consistent with the milder hearing phenotype of *Atp6v1b2*^{Arg506*/Arg506*} mice despite the presence of the same type of mutation (Menendez et al. 2017). Based on the finding that hair cells were not affected in *Atp6v1b2*^{Arg506*/Arg506*} mice, we hypothesized the presence of genetic compensation. Genetic compensation was already shown between isoforms of V-ATPases. For example, compensation exists between *Atp6v1g1* and *Atp6v1g2*, both of which encode the V1G subunit. The V1G subunit plays an important role in the nervous system. Defects in the V1G subunit can lead to cognitive disorders. However, *Atp6v1g2*^{-/-} mice did not show any developmental defects or obvious behavioral abnormalities until adulthood, which is considered to be associated with the upregulation of *Atp6v1g1* in the mouse brain (Kawamura et al. 2015).

The V1B subunits of the V-ATPase are encoded by *Atp6v1b2* and *Atp6v1b1*. *Atp6v1b2* mRNA is ubiquitously expressed in mouse tissues, including the inner ears. *Atp6v1b1* is mainly expressed in the kidney, epididymis, eyes, and inner ears (Tian et al. 2017). The B2 subunit of V-ATPase was shown to compensate for the function of the B1 subunit of V-ATPase in the renal medullary intercalated cells of B1-deficient mice (Paunescu et al. 2007). In this study, we observed increased transcription of *Atp6v1b1* in hair cells of *Atp6v1b2*^{Arg506*/Arg506*} mice and inferred that *Atp6v1b1* compensated for the *Atp6v1b2* dysfunction by increasing its own transcription level. Genetic compensation in hair cells explains the

milder hearing impairment in *Atp6v1b2*^{Arg506*/Arg506*} mice. The mechanism of elevated transcription may be due to an enhancement in the promoter region of the gene by trimethylation (El-Brolosy et al. 2019; Ma et al. 2019). However, if a mutation occurs only at the transcriptome level and not at the DNA level, this compensatory mechanism will not be activated (Ma et al. 2019; Rossi et al. 2015). This finding was verified by our previous work: when we injected morpholinos designed to knock down *Atp6v1b2* mRNA in the cochlea of mice, the hair cells were damaged, and the mice showed severe hearing loss (Yuan et al. 2014).

Conclusions

Based on the findings of this study and our previous studies, we elucidated the pathogenesis of *Atp6v1b2* defects as follows: 1) the mutation causes dysfunctional assembly between V-ATPase V1 subunits, and H⁺ transfer to lysosomes is decreased, which leads to an increased pH value; 2) disequilibrium in the acidic environment of the lysosome further affects the function of acid-dependent hydrolytic enzymes, resulting in the accumulation of degradation substrates; 3) the Bcl-2 family detects abnormal lysosome autophagy and then induces the release of cytochrome C from the mitochondria; and 4) apoptosis occurs in SGNs, affecting hearing function (Fig. 6).

Declarations

Acknowledgements

This study was supported by grants from National Key Research and Development Project of China (2016YFC1000706) and National Natural Science Foundation of China (81873704) and Fostering Funds of Chinese PLA General Hospital for National Distinguished Young Scholar Science Fund (2017-JQPY-001) to Yongyi Yuan, National Key Research and Development Project (2016YFC1000700, 2016YFC1000704) and National Natural Science Foundation of China (81730029) to Pu Dai. Grants from Beijing Natural Science Foundation (7192234) to Xue Gao. The funders had no role in study design, data collection and analysis, decision to publish, or preparation of the manuscript.

Conflict of interests

The authors declare no competing interests.

Authors' contributions

Shiwei Qiu, Weihao Zhao and Yongyi Yuan drafted the manuscript. Shiwei Qiu and Weihao Zhao participated in the construction and analysis of *Atp6v1b2* c.1516C>T knockin mice and performed western blotting, electron microscopy, RNAscope and BIP-V5 treatment. Dapeng Li and Bo Gao carried out the experiments of immunohistochemistry. Xue Gao and Weiqian Wang did the auditory evaluation and statistical analysis. Yongyi Yuan and Pu Dai conceived the study. Peng Cao, Shiming Yang and Weiju Han participated in its design and coordination. All authors have read and approved the final manuscript.

Availability of Data and Materials

All data are presented in the manuscript or Additional files.

References

- Beauregard-Lacroix E, Pacheco-Cuellar G, Ajeawung NF, Tardif J, Dieterich K, Dabir T, Vind-Kezunovic D, White SM, Zadori D, Castiglioni C, Tranebjaerg L, Topping PM, Blair E, Wisniewska M, Camurri MV, van Bever Y, Molidperee S, Taylor J, Dionne-Laporte A, Sisodiya SM, Hennekam RCM, Campeau PM (2020) DOORS syndrome and a recurrent truncating ATP6V1B2 variant. *Genet Med*. doi: 10.1038/s41436-020-00950-9
- Beyenbach KW, Wieczorek H (2006) The V-type H⁺ ATPase: molecular structure and function, physiological roles and regulation. *J Exp Biol* 209: 577-89. doi: 10.1242/jeb.02014
- Bharadwaj HM, Verhulst S, Shaheen L, Liberman MC, Shinn-Cunningham BG (2014) Cochlear neuropathy and the coding of supra-threshold sound. *Front Syst Neurosci* 8: 26. doi: 10.3389/fnsys.2014.00026
- Cerri S, Blandini F (2019) Role of Autophagy in Parkinson's Disease. *Curr Med Chem* 26: 3702-3718. doi: 10.2174/0929867325666180226094351
- Colacurcio DJ, Nixon RA (2016) Disorders of lysosomal acidification-The emerging role of v-ATPase in aging and neurodegenerative disease. *Ageing Res Rev* 32: 75-88. doi: 10.1016/j.arr.2016.05.004
- De Duve C (1957) [The lysosomes: a novel group of cytoplasmic granules]. *J Physiol (Paris)* 49: 113-5.
- El-Brolosy MA, Kontarakis Z, Rossi A, Kuenne C, Gunther S, Fukuda N, Kikhi K, Boezio GLM, Takacs CM, Lai SL, Fukuda R, Gerri C, Giraldez AJ, Stainier DYR (2019) Genetic compensation triggered by mutant mRNA degradation. *Nature* 568: 193-197. doi: 10.1038/s41586-019-1064-z
- Fischer N, Johnson Chacko L, Glueckert R, Schrott-Fischer A (2019) Age-Dependent Changes in the Cochlea. *Gerontology*: 1-7. doi: 10.1159/000499582
- Galluzzi L, Vitale I, Abrams JM, Alnemri ES, Baehrecke EH, Blagosklonny MV, Dawson TM, Dawson VL, El-Deiry WS, Fulda S, Gottlieb E, Green DR, Hengartner MO, Kepp O, Knight RA, Kumar S, Lipton SA, Lu X, Madeo F, Malorni W, Mehlen P, Nunez G, Peter ME, Piacentini M, Rubinsztein DC, Shi Y, Simon HU, Vandenabeele P, White E, Yuan J, Zhivotovsky B, Melino G, Kroemer G (2012) Molecular definitions of cell death subroutines: recommendations of the Nomenclature Committee on Cell Death 2012. *Cell Death Differ* 19: 107-20. doi: 10.1038/cdd.2011.96
- Hughes AL, Gottschling DE (2012) An early age increase in vacuolar pH limits mitochondrial function and lifespan in yeast. *Nature* 492: 261-5. doi: 10.1038/nature11654

- Ilmarinen P, Moilanen E, Kankaanranta H (2014) Mitochondria in the center of human eosinophil apoptosis and survival. *Int J Mol Sci* 15: 3952-69. doi: 10.3390/ijms15033952
- Kawamura N, Sun-Wada GH, Wada Y (2015) Loss of G2 subunit of vacuolar-type proton transporting ATPase leads to G1 subunit upregulation in the brain. *Sci Rep* 5: 14027. doi: 10.1038/srep14027
- Kortum F, Caputo V, Bauer CK, Stella L, Ciolfi A, Alawi M, Bocchinfuso G, Flex E, Paolacci S, Dentici ML, Grammatico P, Korenke GC, Leuzzi V, Mowat D, Nair LD, Nguyen TT, Thierry P, White SM, Dallapiccola B, Pizzuti A, Campeau PM, Tartaglia M, Kutsche K (2015) Mutations in KCNH1 and ATP6V1B2 cause Zimmermann-Laband syndrome. *Nat Genet* 47: 661-7. doi: 10.1038/ng.3282
- Kroemer G, Galluzzi L, Brenner C (2007) Mitochondrial membrane permeabilization in cell death. *Physiol Rev* 87: 99-163. doi: 10.1152/physrev.00013.2006
- Kujawa SG, Liberman MC (2009) Adding insult to injury: cochlear nerve degeneration after "temporary" noise-induced hearing loss. *J Neurosci* 29: 14077-85. doi: 10.1523/JNEUROSCI.2845-09.2009
- Liberman MC, Kujawa SG (2017) Cochlear synaptopathy in acquired sensorineural hearing loss: Manifestations and mechanisms. *Hear Res* 349: 138-147. doi: 10.1016/j.heares.2017.01.003
- Liu H, Lu J, Wang Z, Song L, Wang X, Li GL, Wu H (2019) Functional alteration of ribbon synapses in inner hair cells by noise exposure causing hidden hearing loss. *Neurosci Lett* 707: 134268. doi: 10.1016/j.neulet.2019.05.022
- Liu K, Chen D, Guo W, Yu N, Wang X, Ji F, Hou Z, Yang WY, Yang S (2015) Spontaneous and Partial Repair of Ribbon Synapse in Cochlear Inner Hair Cells After Ototoxic Withdrawal. *Mol Neurobiol* 52: 1680-1689. doi: 10.1007/s12035-014-8951-y
- Ma B, Xiang Y, An L (2011) Structural bases of physiological functions and roles of the vacuolar H(+)-ATPase. *Cell Signal* 23: 1244-56. doi: 10.1016/j.cellsig.2011.03.003
- Ma Z, Zhu P, Shi H, Guo L, Zhang Q, Chen Y, Chen S, Zhang Z, Peng J, Chen J (2019) PTC-bearing mRNA elicits a genetic compensation response via Upf3a and COMPASS components. *Nature* 568: 259-263. doi: 10.1038/s41586-019-1057-y
- Mauvezin C, Nagy P, Juhasz G, Neufeld TP (2015) Autophagosome-lysosome fusion is independent of V-ATPase-mediated acidification. *Nat Commun* 6: 7007. doi: 10.1038/ncomms8007
- Mehraei G, Hickox AE, Bharadwaj HM, Goldberg H, Verhulst S, Liberman MC, Shinn-Cunningham BG (2016) Auditory Brainstem Response Latency in Noise as a Marker of Cochlear Synaptopathy. *J Neurosci* 36: 3755-64. doi: 10.1523/JNEUROSCI.4460-15.2016
- Menendez I, Carranza C, Herrera M, Marroquin N, Foster J, 2nd, Cengiz FB, Bademci G, Tekin M (2017) Dominant deafness-onychodystrophy syndrome caused by an ATP6V1B2 mutation. *Clin Case Rep* 5: 376-

379. doi: 10.1002/ccr3.761

Mindell JA (2012) Lysosomal acidification mechanisms. *Annu Rev Physiol* 74: 69-86. doi: 10.1146/annurev-physiol-012110-142317

Molin M, Demir AB (2014) Linking Peroxiredoxin and Vacuolar-ATPase Functions in Calorie Restriction-Mediated Life Span Extension. *Int J Cell Biol* 2014: 913071. doi: 10.1155/2014/913071

Paunescu TG, Russo LM, Da Silva N, Kovacicova J, Mohebbi N, Van Hoek AN, McKee M, Wagner CA, Breton S, Brown D (2007) Compensatory membrane expression of the V-ATPase B2 subunit isoform in renal medullary intercalated cells of B1-deficient mice. *Am J Physiol Renal Physiol* 293: F1915-26. doi: 10.1152/ajprenal.00160.2007

Peric A, Annaert W (2015) Early etiology of Alzheimer's disease: tipping the balance toward autophagy or endosomal dysfunction? *Acta Neuropathol* 129: 363-81. doi: 10.1007/s00401-014-1379-7

Rasband MN, Peles E (2015) The Nodes of Ranvier: Molecular Assembly and Maintenance. *Cold Spring Harb Perspect Biol* 8: a020495. doi: 10.1101/cshperspect.a020495

Rossi A, Kontarakis Z, Gerri C, Nolte H, Holper S, Kruger M, Stainier DY (2015) Genetic compensation induced by deleterious mutations but not gene knockdowns. *Nature* 524: 230-3. doi: 10.1038/nature14580

Ruckenstuhl C, Netzberger C, Entfellner I, Carmona-Gutierrez D, Kickenweiz T, Stekovic S, Gleixner C, Schmid C, Klug L, Sorgo AG, Eisenberg T, Buttner S, Marino G, Koziel R, Jansen-Durr P, Frohlich KU, Kroemer G, Madeo F (2014) Lifespan extension by methionine restriction requires autophagy-dependent vacuolar acidification. *PLoS Genet* 10: e1004347. doi: 10.1371/journal.pgen.1004347

Saftig P, Haas A (2016) Turn up the lysosome. *Nat Cell Biol* 18: 1025-7. doi: 10.1038/ncb3409

Shrestha BR, Chia C, Wu L, Kujawa SG, Liberman MC, Goodrich LV (2018) Sensory Neuron Diversity in the Inner Ear Is Shaped by Activity. *Cell* 174: 1229-1246 e17. doi: 10.1016/j.cell.2018.07.007

Song MH, Jung J, Rim JH, Choi HJ, Lee HJ, Noh B, Lee JS, Gee HY, Choi JY (2019) Genetic Inheritance of Late-Onset, Down-Sloping Hearing Loss and Its Implications for Auditory Rehabilitation. *Ear Hear*. doi: 10.1097/AUD.0000000000000734

Sun S, Babola T, Pregernig G, So KS, Nguyen M, Su SM, Palermo AT, Bergles DE, Burns JC, Muller U (2018) Hair Cell Mechanotransduction Regulates Spontaneous Activity and Spiral Ganglion Subtype Specification in the Auditory System. *Cell* 174: 1247-1263 e15. doi: 10.1016/j.cell.2018.07.008

Tian C, Gagnon LH, Longo-Guess C, Korstanje R, Sheehan SM, Ohlemiller KK, Schrader AD, Lett JM, Johnson KR (2017) Hearing loss without overt metabolic acidosis in ATP6V1B1 deficient MRL mice, a

new genetic model for non-syndromic deafness with enlarged vestibular aqueducts. *Hum Mol Genet* 26: 3722-3735. doi: 10.1093/hmg/ddx257

Vreugde S, Erven A, Kros CJ, Marcotti W, Fuchs H, Kurima K, Wilcox ER, Friedman TB, Griffith AJ, Balling R, Hrabe De Angelis M, Avraham KB, Steel KP (2002) Beethoven, a mouse model for dominant, progressive hearing loss DFNA36. *Nat Genet* 30: 257-8. doi: 10.1038/ng848

Wan G, Corfas G (2017) Transient auditory nerve demyelination as a new mechanism for hidden hearing loss. *Nat Commun* 8: 14487. doi: 10.1038/ncomms14487

Yuan Y, Zhang J, Chang Q, Zeng J, Xin F, Wang J, Zhu Q, Wu J, Lu J, Guo W, Yan X, Jiang H, Zhou B, Li Q, Gao X, Yuan H, Yang S, Han D, Mao Z, Chen P, Lin X, Dai P (2014) De novo mutation in ATP6V1B2 impairs lysosome acidification and causes dominant deafness-onychodystrophy syndrome. *Cell Res* 24: 1370-3. doi: 10.1038/cr.2014.77

cr201477 [pii]

Zhao W, Gao X, Qiu S, Gao B, Gao S, Zhang X, Kang D, Han W, Dai P, Yuan Y (2019) A subunit of V-ATPases, ATP6V1B2, underlies the pathology of intellectual disability. *EBioMedicine* 45: 408-421. doi: S2352-3964(19)30415-3 [pii]

10.1016/j.ebiom.2019.06.035

Figures

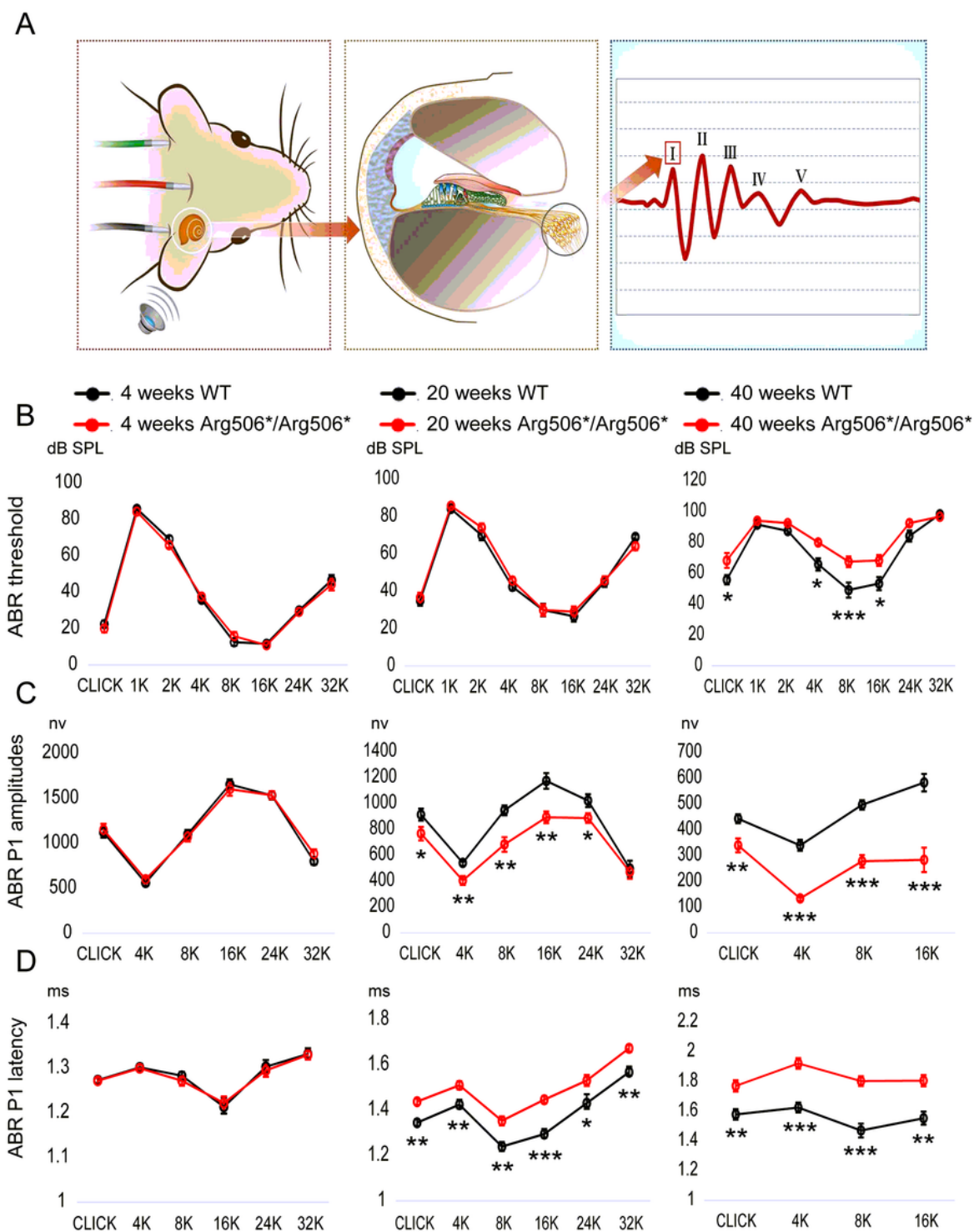


Figure 1

Progressive hearing impairment with increasing age in *Atp6v1b2Arg506*/Arg506** mice. (A) Auditory brainstem responses (ABR) were recorded to evaluate the hearing in mice. After acoustic stimulation, the recording electrode recorded five waveforms, of which peak I (P1) was derived from spiral ganglion neurons in the mouse cochlea. The hearing thresholds were defined as the lowest sound intensity that elicited identifiable waves. (B) ABR thresholds (shown in ordinate) to click and to 1, 2, 4, 8, 16, 24, and 32

kHz (shown in abscissa) tone-burst stimuli were compared between WT and Atp6v1b2Arg506*/Arg506* mice. At 4 weeks and 20 weeks, ABR thresholds showed no significant difference between WT and Atp6v1b2Arg506*/Arg506* mice. At 40 weeks, ABR thresholds to click and to 4, 8, and 16 kHz stimuli were significantly higher in Atp6v1b2Arg506*/Arg506* than in WT mice. (C) ABR P1 amplitudes (shown in ordinate) were compared between WT and Atp6v1b2Arg506*/Arg506* mice. There was no significant difference at 4 weeks. At 20 weeks, Atp6v1b2Arg506*/Arg506* mice had significantly lower peaks to click and to 4, 8, 16 and 24 kHz tone-burst stimuli than WT mice. At 40 weeks, Atp6v1b2Arg506*/Arg506* mice had significantly lower peaks to click and to 4, 8, and 16 kHz tone-burst stimuli than WT mice. (D) ABR P1 latencies (shown in ordinate) stimulated by different sound types (shown in abscissa) with the same sound intensity (90 dB SPL) were compared between WT and Atp6v1b2Arg506*/Arg506* mice. There was no significant difference at 4 weeks. At 20 weeks, Atp6v1b2Arg506*/Arg506* mice showed significantly longer latencies to click and to 4, 8, 16, 24 and 32 kHz tone-burst stimuli than WT mice. At 40 weeks, Atp6v1b2Arg506*/Arg506* mice showed significantly longer latencies to click and to 4, 8, and 16 kHz tone-burst stimuli than WT mice. The t-test was performed to evaluate statistical significance; n represents the number of test ears, n=6 for each group; * denotes $P < 0.05$, ** denotes $P < 0.01$, *** denotes $P < 0.001$. Data are described as mean + SEM (standard error of mean).

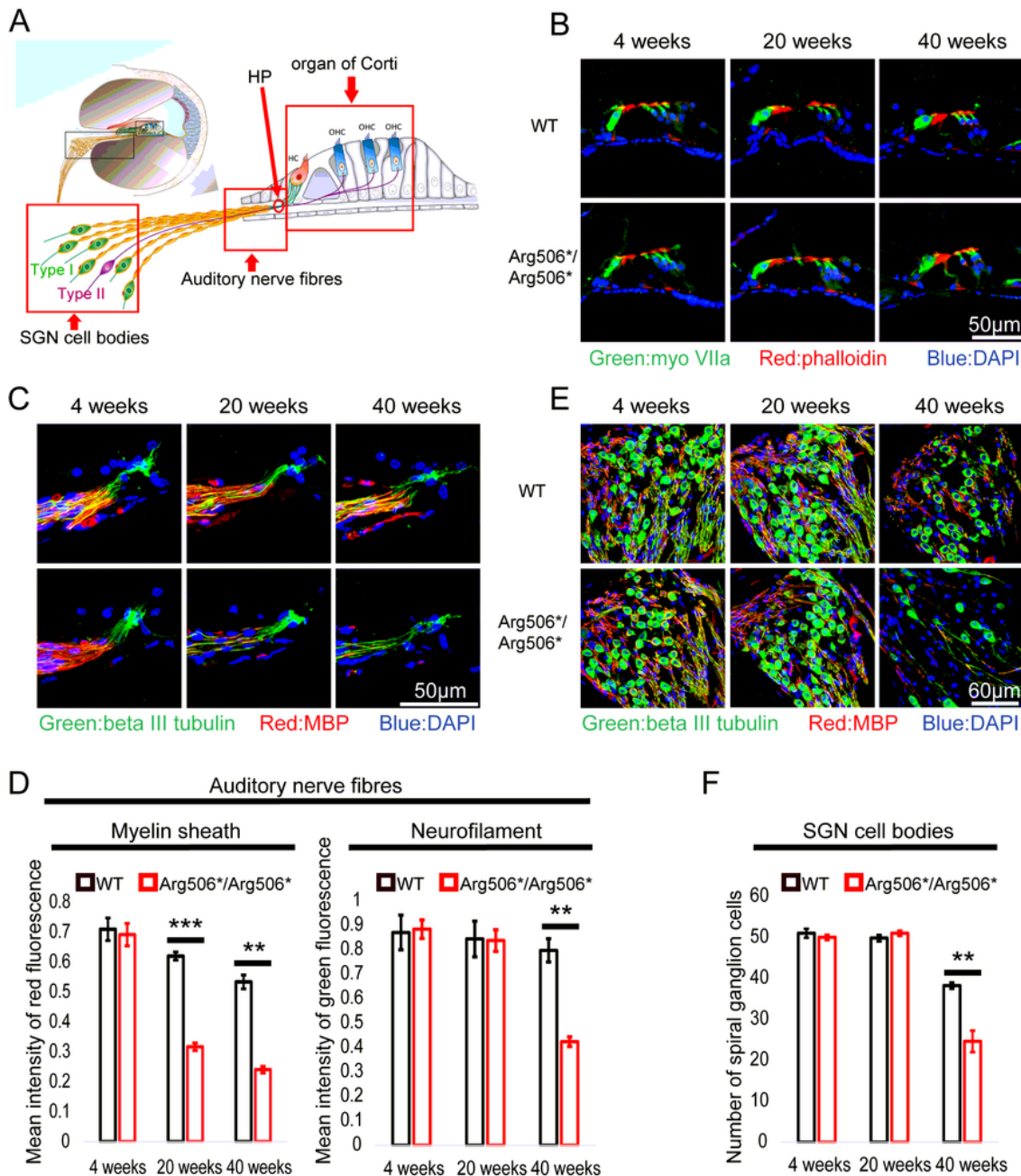


Figure 2

Abnormal morphology in the cochlea of *Atp6v1b2Arg506*/Arg506** mice at different postnatal ages of 4, 20, and 40 weeks. (A) Illustration of the cochlear architecture. The three areas within the red frame (from left to right): spiral ganglion neuron (SGN) cell bodies, auditory nerve fibers, and organ of Corti. (B) There is no obvious difference in the morphology of organ of Corti between WT and *Atp6v1b2Arg506*/Arg506** mice. Phalloidin, Myo VIIa, and DAPI are markers of hair cell cilia, inner/outer hair cells, and nuclei,

respectively. The experiments were repeated three times. (C) Representative images of auditory nerve fibers for WT and *Atp6v1b2Arg506*/Arg506** mice. (D) Statistical results of the red and green fluorescence intensities for Figure 2C. The intensity of red fluorescence (myelin) decreased significantly at 20 and 40 weeks in *Atp6v1b2Arg506*/Arg506** mice. The intensity of green fluorescence (nerve fibers) decreased significantly at 40 weeks in *Atp6v1b2Arg506*/Arg506** mice. (E) Representative images of SGN cell bodies of WT and *Atp6v1b2Arg506*/Arg506** mice. (F) Statistical results of the number of SGN cell bodies for Figure 2E. The number of SGN cell bodies decreased significantly in *Atp6v1b2Arg506*/Arg506** mice compared to that in WT mice at 40 weeks. The myelin sheath, nerve fibers, and nuclei are labeled with red (MBP), green (beta III tubulin), and blue (DAPI) fluorescence, respectively. The t-test was performed to evaluate the statistical significance. Each group included three mice, and one slice for each mouse was processed. ** denotes $P < 0.01$, *** denotes $P < 0.001$. Data are described as mean \pm SEM (standard error of mean). HP, habenula perforate.

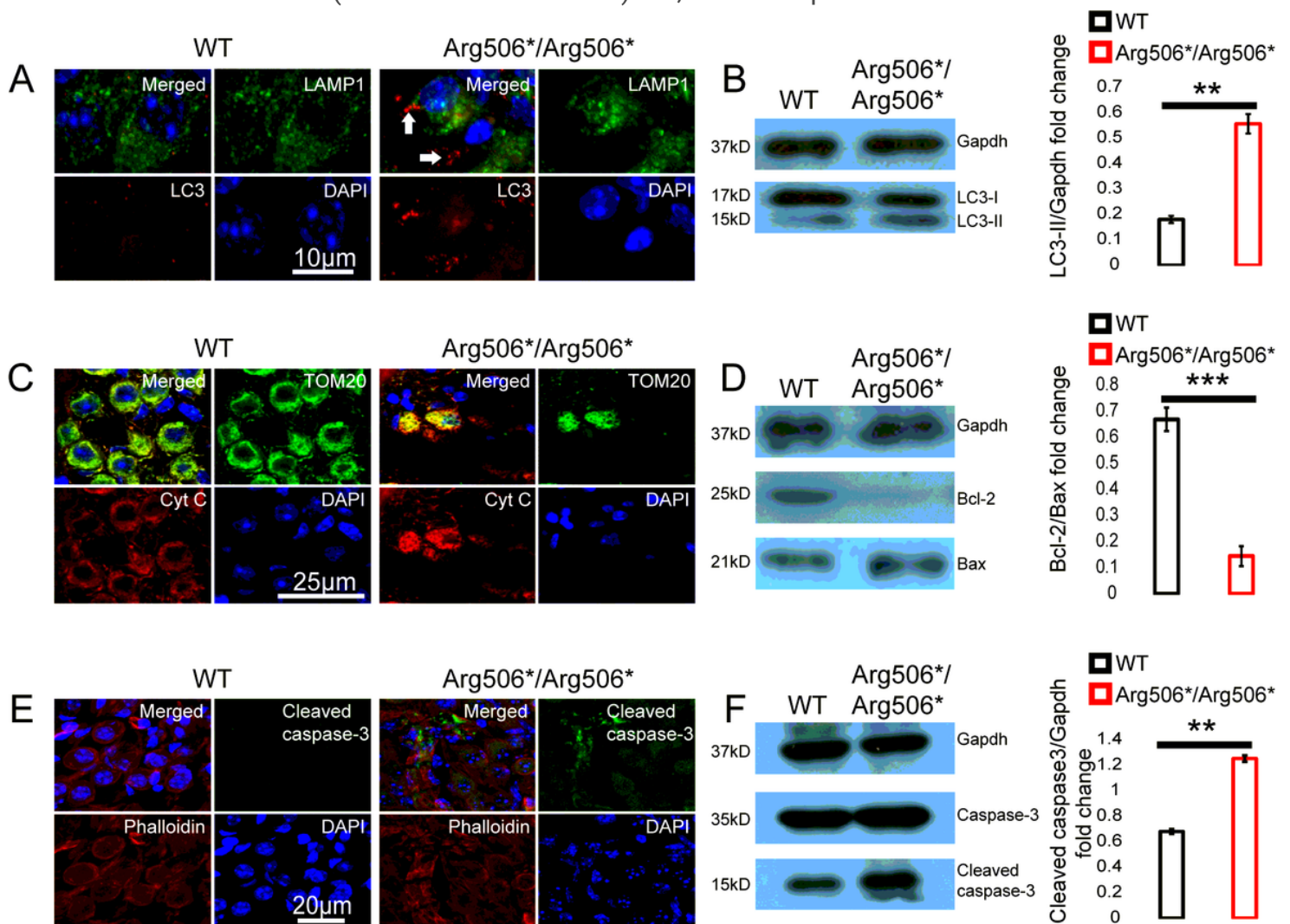


Figure 3

Abnormal autophagy and apoptosis activated by cytochrome C in the spiral ganglion neurons (SGNs) of *Atp6v1b2Arg506*/Arg506** mice. (A) Representative images of immunostaining showed that autophagosomes labeled with LC3 (white arrows) were present in large numbers as dots in the SGNs of

Atp6v1b2Arg506*/Arg506* mice. (B) Left: Western blotting results showed that LC3-II increased in the cochlea of Atp6v1b2Arg506*/Arg506* mice compared with that in the cochlea of WT mice. LC3-II can be used to estimate the extent of autophagy. Right: Statistical results of gray value for western blotting. The ratio of LC3-II/Gapdh in the cochlea of Atp6v1b2Arg506*/Arg506* mice was significantly higher than that in the cochlea of WT mice (** denotes $P < 0.01$ by t-test; $n = 3$ for each group). (C) The release of cytochrome C from the mitochondria into the cytosol of the SGNs in Atp6v1b2Arg506*/Arg506* mice is shown. Mitochondria are labeled with TOM20 (green). Cytochrome C is labeled as red. In WT mice, cytochrome C remains in the mitochondria and no red signal was observed in the cytosol of the SGNs. In Atp6v1b2Arg506*/Arg506* mice, cytochrome C was observed both in the mitochondria and the cytosol of the SGNs, indicating its release from mitochondria. (D) Left: Western blotting results showed that in the cochlea of Atp6v1b2Arg506*/Arg506* mice, Bcl-2 decreased significantly compared with that in the cochlea of WT mice. Right: Statistical results of gray value for western blotting (***) denotes $P < 0.001$ by t-test; $n = 3$ for each group). (E) More pronounced positive signal for cleaved caspase-3 in the region of SGNs of Atp6v1b2Arg506*/Arg506* mice was identified. Phalloidin is a high-affinity filamentous actin (F-actin) marker, which is used to mark the cytoskeleton. (F) Left: Western blotting results showed that cleaved caspase-3 increased in the cochlea of Atp6v1b2Arg506*/Arg506* mice compared with that in the cochlea of WT mice. Right: Statistical results of gray value for western blotting. The ratio of cleaved caspase-3/Gapdh in the cochlea of Atp6v1b2Arg506*/Arg506* mice was significantly higher than that in the cochlea of WT mice. ** denotes $P < 0.01$. $n = 3$ for each group. Data are described as mean \pm SEM (standard error of mean). Cyt C, cytochrome C.

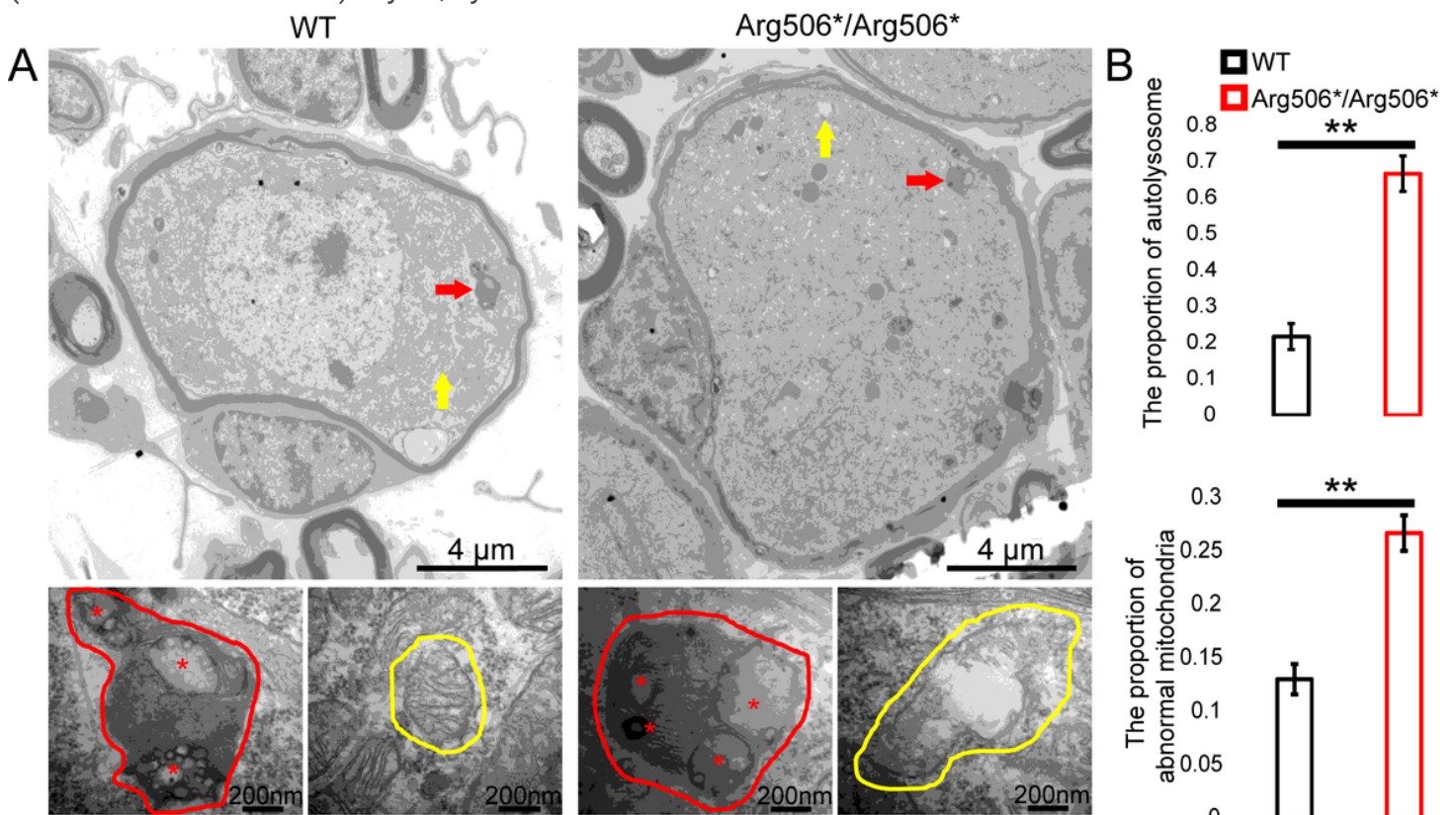


Figure 4

Transmission electron microscopy images of the organelles of SGNs in *Atp6v1b2Arg506*/Arg506** and WT mice. (A) Red arrows and red circles indicate the locations and enlarged views of a typical autophagy lysosome, respectively. Yellow arrows and yellow circles indicate the locations and enlarged views of mitochondria, respectively. In *Atp6v1b2Arg506*/Arg506** mice, increased degraded substrates indicated by red asterisks in the autophagy lysosomes of the spiral ganglion neurons (SGNs) were observed, and some of the mitochondria appeared swollen. Most of the mitochondria in the SGNs showed normal morphology in WT mice. (B) The percentage of autolysosomes and abnormal mitochondria significantly increased in *Atp6v1b2Arg506*/Arg506** mice. The t-test was performed to evaluate statistical significance. The percentage of autolysosomes in lysosomes and the percentage of abnormal mitochondria were manually determined. Each group included three mice, and one slice for each mouse was processed. Data are described as mean \pm SEM (standard error of mean). ** denotes $P < 0.01$.

RNAscope

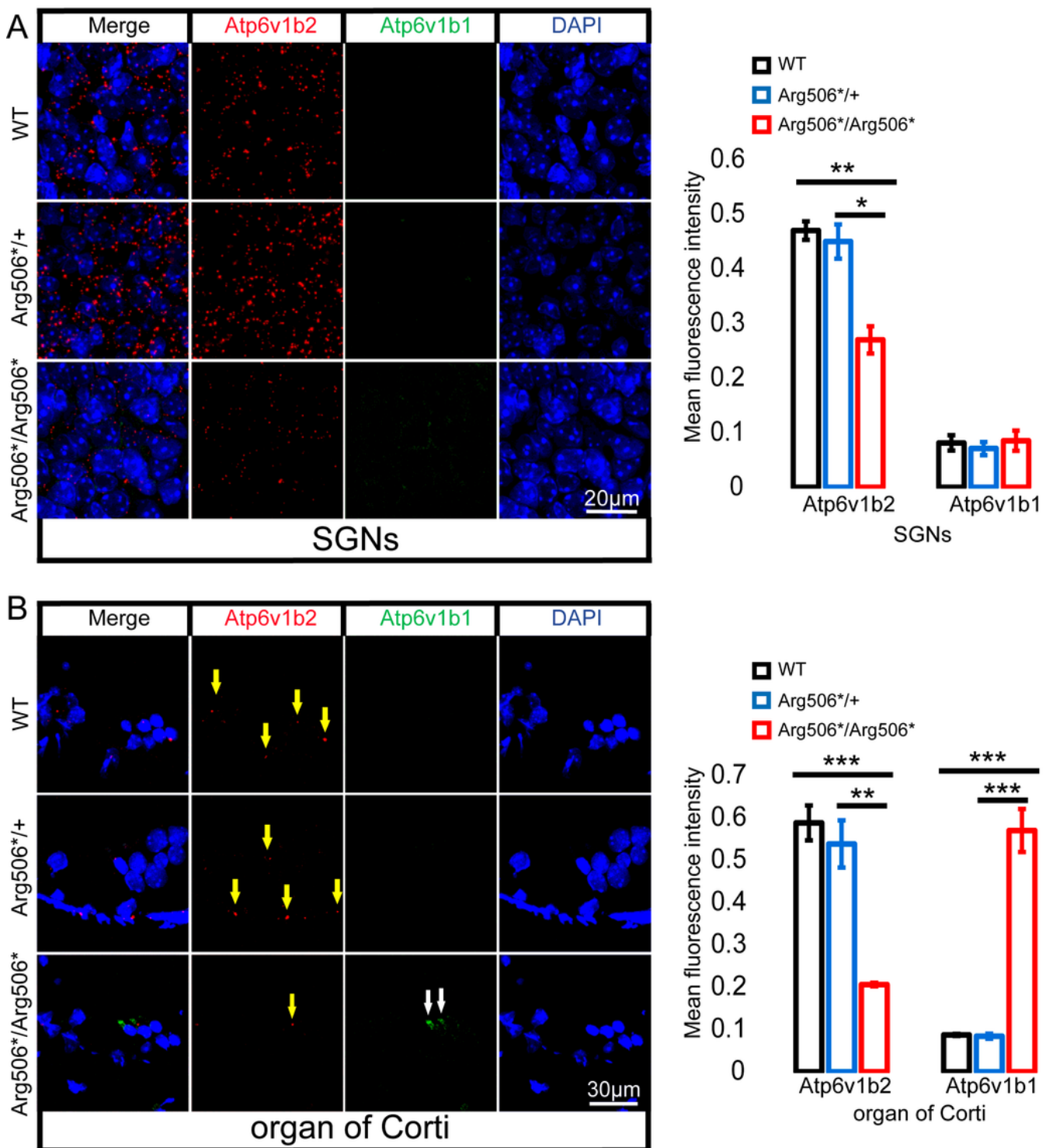


Figure 5

Increased transcription of *Atp6v1b1* occurs in the hair cells of *Atp6v1b2Arg506^{*/Arg506*}* mice. (A) Representative images and quantification of RNAscope results in the spiral ganglion neurons (SGNs). The mean fluorescence intensity of *Atp6v1b2* RNA in *Atp6v1b2Arg506^{*/Arg506*}* mice was significantly lower than that in WT and *Atp6v1b2Arg506^{*/+}* mice. No *Atp6v1b1* RNA was found in the SGNs. (B) Representative images and quantification of RNAscope results in the organ of Corti. *Atp6v1b2* RNA

decreased in *Atp6v1b2Arg506*/Arg506** mice compared with that in WT and *Atp6v1b2Arg506*/+* mice (yellow arrow). There was no significant difference in the mean fluorescence intensity of *Atp6v1b2* RNA between WT and *Atp6v1b2Arg506*/+* mice. *Atp6v1b1* RNA was found in the hair cells of *Atp6v1b2Arg506*/Arg506** mice (white arrow) but not in the hair cells of WT and *Atp6v1b2Arg506*/+* mice. $n=3$ for each group. * denotes $P<0.05$, ** denotes $P<0.01$ and *** denotes $P<0.001$. Data are described as mean \pm SEM (standard error of mean).

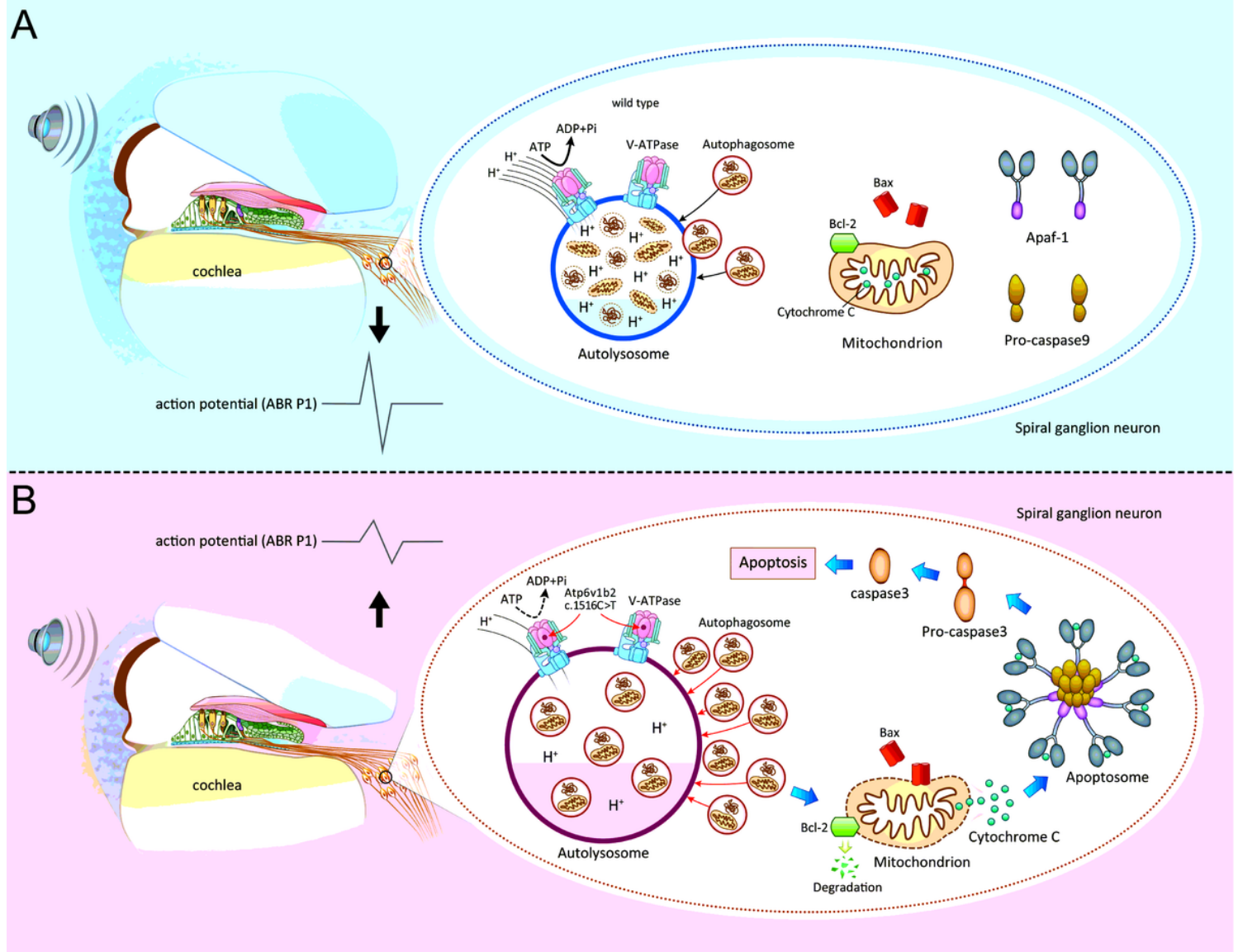


Figure 6

Apoptosis induced by lysosome dysfunction and autophagic flux block in spiral ganglion neurons (SGNs) causes hearing impairment in *Atp6v1b2Arg506*/Arg506** mice. (A) In WT mice, V-ATPases in the SGNs maintain the acidic environment by pumping protons into the lumen of lysosomes. It is a process that requires ATP hydrolysis. When autophagosomes enter the lysosomes, the intracellular components carried by autophagosomes are degraded. The magnitude of peak I (P1) amplitudes of ABR correlates with the number and synchronous firing rate of the SGN fibers. (B) *Atp6v1b2* c.1516 C>T affects the assembly of V-ATPases and their role in pumping protons into the lumen of lysosomes. Thus, the pH in

the lysosomes increases, and the activity of acid hydrolases decreases. Under this circumstance, the autophagosomes are not effectively degraded and they accumulate in the lysosomes, which further affects the entrance of other autophagosomes. When the anti-apoptotic member of Bcl-2 family, Bcl-2, detects the acid environment disequilibrium in the lysosomes and autophagosome accumulation within the cytoplasm, it itself degrades, which in turn activates Bax/Bak complexes. Bax binds to and decreases the permeability of the mitochondrial membrane, leading to cytochrome C release. Cytochrome C binds to its partner Apaf-1 to induce the formation of a caspase-9-activating protein complex known as an apoptosome, which directly activates caspase-3, the ultimate initiator of the apoptosis process. Once apoptosis occurs in the SGNs, the hearing is impaired.

Supplementary Files

This is a list of supplementary files associated with this preprint. Click to download.

- [FigureS1.tif](#)
- [FigureS2.tif](#)
- [FigureS3.tif](#)
- [FigureS4.tif](#)
- [figureS5.tif](#)
- [figureS6.tif](#)
- [figureS7.tif](#)